ACS Catalysis

Research Article

pubs.acs.org/acscatalysis

Degradation Mechanisms of Pt/C Fuel Cell Catalysts under Simulated Start–Stop Conditions

Josef C. Meier,*[,†,§] Carolina Galeano,[⊥] Ioannis Katsounaros,[†] Angel A. Topalov,[†,§] Aleksander Kostka,[‡] Ferdi Schüth,[⊥] and Karl J. J. Mayrhofer*[,†]

[†]Department of Interface Chemistry and Surface Engineering and [‡]Department of Microstructure Physics and Alloy Design, Max-Planck-Institut für Eisenforschung, Max-Planck-Strasse 1, 40237 Düsseldorf, Germany

[§]Center for Electrochemical Sciences, Ruhr-Universität Bochum, Universitätsstrasse 150, 44780 Bochum, Germany

[⊥]Department of Heterogeneous Catalysis, Max-Planck-Institut für Kohlenforschung, Kaiser-Wilhelm-Platz 1, 45470 Mülheim an der Ruhr, Germany

Supporting Information Web-Enhanced

ABSTRACT: This manuscript investigates the degradation of a Pt/Vulcan fuel cell catalyst under simulated start–stop conditions in an electrochemical half-cell. Identical location transmission electron microscopy (IL-TEM) is used to visualize the several different degradation pathways occurring on the same catalyst material under potential cycling conditions. The complexity of degradation on the nanoscale leading to macroscopic active surface area loss is demonstrated and discussed. Namely, four different degradation pathways at one single Pt/Vulcan aggregate are clearly observed. Furthermore, inhomogeneous degradation behavior for different catalyst locations is shown, and trends in degradation mechanisms related to the platinum particle size are discussed in brief. Attention is drawn to the vast field of parameters influencing catalyst stability. We also present the development of a new technique to study changes of the catalyst not only with 2D projections of standard TEM images but also in 3D. For this purpose, identical location tomography (IL-tomography) is introduced, which visualizes the 3D structure of an identical catalyst location before and after degradation.

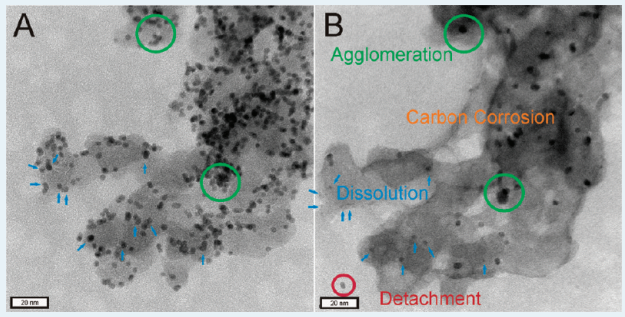

KEYWORDS: *fuel cell, catalyst degradation, degradation mechanism, transmission electron microscopy, electron tomography, IL-TEM, IL-tomography*

INTRODUCTION

The growing demand for alternative energy conversion systems to substitute for combustion engines is currently giving a strong boost to the field of electrocatalysis. Within this discipline, electrode catalysts for proton exchange membrane fuel cells (PEMFCs) are among the most promising and challenging subjects of research. State-of-the-art low-temperature fuel cell electrode catalysts for the anode as well as the cathode are typically based on platinum nanoparticles supported on a carbon support. In recent decades, the research has been focused mainly on understanding and improving the activity of such catalysts, in particular, for the performance-limiting oxygen reduction reaction (ORR). For instance, the important influence of the particle size and of alloying platinum with transition metals on the ORR activity are two topics that have been extensively studied and have led to significant improvements.[1−7] However, not only is the efficiency of a fuel cell linked to the activity of its catalyst at the beginning of its lifetime, but also the catalyst needs to maintain this and other decisive features during the complete lifecycle of several thousands of hours. Especially at the cathode side, where the catalyst is exposed to the most drastic operating conditions, the stability of catalysts is a crucial prerequisite for high-performance fuel cells.

The degradation of platinum nanoparticles supported on a carbon material is strongly dependent on the structure and composition of the support as well as the operating conditions. A highly complex field of parameters is spanned around support and platinum properties, such as platinum loading, particle size, or spatial particle distribution, and the respective working electrode potentials, temperature, pH, and impurities as just some of the most important factors. A variety of helpful summaries on fuel cell stability in general[8−10] and electrode catalyst stability in particular[11−13] provide an excellent overview of these aspects. A clear link among all of these parameters and their influence on the kinetics of individual degradation mechanisms, however,

Special Issue: Electrocatalysis

Received: January 13, 2012
Revised: March 15, 2012
Published: March 27, 2012

is still missing and needs to be established to develop strategies to improve the catalyst stability.

The dynamics during start−stop cycles of fuel cells were found to be extremely harmful to the catalyst and often have a dominant influence on its durability.[8,10,12] The main reason for the catalyst degradation is that the cathode potential can locally rise to values up to 1.5 V during the initial phase when the fuel gas purging is insufficient, causing aging of the carbon support as well as the platinum nanoparticles.[8,12,14] Moreover, as demonstrated by Kinoshita et al., catalyst deterioration is especially severe when the electrode potential is actively changing, in contrast to rather static operating potentials.[15]

The prevailing degradation mechanisms under these specific start−stop conditions are only poorly understood, because of the inherent complexity of a multicomponent fuel cell system. To obtain precise and reliable information about catalyst degradation and exclusively study the intrinsic stability of the cathode catalyst, ex-situ investigations in electrochemical cells are a very useful approach. Such tests are faster than fuel cell tests and allow better control of the degradation conditions to which the catalyst is subjected. Potential fluctuations during start−stop conditions can be readily simulated via controlled fast potential cycling experiments, leading to very rapid degradation in a short period of time. Such experiments are therefore also called "accelerated aging tests".[12] Moreover, complementary imaging techniques, such as identical location transmission electron microscopy (IL-TEM), can be utilized, which provide insight into the exact degradation mechanisms caused by the accelerated aging tests.[16,17]

In this work, we investigate the degradation mechanisms taking place at a standard fuel cell catalyst with platinum nanoparticles supported on a Vulcan carrier under simulated start−stop conditions. The complexity of the degradation processes is revealed by the simultaneous action of different mechanisms occurring at the same catalyst aggregates. Because TEM is able to provide only 2D information, we additionally extend the concept of IL-TEM to 3D imaging. For this purpose, for the first time, we apply electron tomography at identical catalyst locations before and after simulated start−stop conditions, which is hereafter referred to as identical location tomography (IL-tomography).

EXPERIMENTAL SECTION

Catalyst Material. Pt supported on Vulcan XC72R was prepared via a colloidal deposition method.[18] Colloidal deposition allows the formation of platinum particles, which are highly uniform in size and shape. The platinum colloids were prepared by the polyol route using ethylene glycol as solvent/reductant.[19] Typically, K_2PtCl_4 (80 mg, 0.2 mmol, Sigma-Aldrich, 99.9% trace metal basis) and polyvinylpyrrolidone (PVP, 57 mg, MW = 55 000, Sigma-Aldrich) were dissolved in 40 mL of ethylene glycol and heated at 50 °C until complete dissolution (~30 min). The completely organic surfactant PVP was employed to avoid working with halides during platinum particle deposition. Subsequently, the solution was refluxed at 190 °C for 3 h. When the colloidal solution had cooled to ambient temperature, the Vulcan support (150 mg, Cabot lot: 6P-3875) was added under vigorous stirring. Afterward, 100 mL of acetone was added, and the suspension was stirred for 12 h. The Pt nanoparticles supported on Vulcan were separated by centrifugation (9000 rpm, 10 min) and dried at 75 °C overnight. Finally, the Pt/Vulcan catalyst was thermally treated at 350 °C under Ar for 10 h to remove the surfactant.

The resulting platinum content was determined via elemental analysis (AAS), thermogravimetric analysis (TGA), and X-ray photoelectron spectroscopy (XPS). A Pt content of 20 wt % was confirmed (Table S1 and Figure S1 in the Supporting Information). Furthermore, XPS was used to determine an oxygen content of 3 wt %. The platinum particle size distribution was investigated via TEM. A monodisperse distribution with an average particle size of 3.6 nm was obtained. The electrochemical surface area (ECSA) was determined to be 71 $m^2\ g^{-1}$, as calculated from CO-stripping experiments (see Electrochemical Measurements).

The Vulcan support material was used as obtained and not pretreated in this study. The highest temperature used in the preparation process was 350 °C for the removal of surfactants. Pretreatment of the support (such as reducing, oxidizing, or heat-treatment conditions; surface functional group modification of the support; etc.) has a significant influence on the degradation behavior[20] and is therefore in the focus of ongoing studies. The non-pretreated Vulcan support in this work acts as a reference system for the investigation of the influence of support pretreatment procedures on the degradation mechanisms in further studies.

Electrochemical Measurements. Suspensions of 0.24 $mg_{Pt}\ cm^{-3}$ of catalyst powder in a mixture of isopropyl alcohol (Merck, pro analysis) and ultrapure water (1:50) were dispersed ultrasonically. Nine microliters of the well dispersed suspension was pipetted onto a glassy carbon disk (0.196 cm^2 geometrical surface area) and then dried under vacuum or air, resulting in a catalyst loading of 11 $\mu g_{Pt}\ cm^{-2}$. The electrochemical measurements were performed at room temperature in a three-compartment, three electrode electrochemical cell made of Teflon only. The Teflon tip containing the carbon disk with a uniform catalyst film was contacted to a rotating disk electrode (Radiometer Analytical, France), which served as the working electrode. A graphite rod was used as the counter electrode; a saturated Ag/AgCl electrode (Metrohm), as reference. The reference was housed in a compartment separate from the main compartment protected with a Nafion membrane to avoid contamination with chlorides during degradation tests. All potentials are given with respect to the reversible hydrogen electrode (RHE) potential, which was determined for each experiment individually. A Gamry reference 600 potentiostat was employed and controlled in combination with the rotator and the gas system with an in-house-developed LabVIEW software.[21] All experiments were carried out with ~150 mL of 0.1 M $HClO_4$ electrolyte. The electrolyte was prepared with ultrapure water (18 MΩ, Millipore) and concentrated $HClO_4$ (Merck, Suprapur). Solution resistance was compensated via positive feedback so that the residual uncompensated resistance was <3 Ω in all experiments.

The accelerated aging test consisted of 10 800 degradation cycles between 0.4 and 1.4 V_{RHE} with a sweep rate of 1 $V\ s^{-1}$. All degradation tests were performed in an argon atmosphere without rotation. CO-stripping voltammograms were recorded after 0, 360, 1080, 2160, 3600, 5400, 7200, and 10 800 cycles for the determination of the active platinum surface area. In each CO-stripping experiment, carbon monoxide is adsorbed on the platinum at a potential at which no CO oxidation occurs (0.05 V_{RHE}). Afterward, the electrolyte is purged with argon again until all remaining carbon monoxide is removed from the electrolyte, while the same potential is held. Finally, preadsorbed CO is oxidized electrochemically by cycling between 0.05 and 1.2 V_{RHE} with a scan rate of 0.05 $V\ s^{-1}$, and the charge corresponding to the CO oxidation is measured by the area of the oxidation peak. More information about surface area

dx.doi.org/10.1021/cs300024h | ACS Catal. 2012, 2, 832−843

determination with anodic CO stripping can be found in the literature.[22]

Identical Location Transmission Electron Microscopy (IL-TEM). For the TEM investigations, the catalyst suspension was diluted by a factor of 1:5 with ultrapure water. About 5 μL of the diluted suspension was loaded at the top side of a gold finder grid (NH2A, Plano) coated with a carbon film (Quantifoil R2/2). To keep the catalyst loading as low as possible (to avoid overlapping catalyst particles), the drop was absorbed off the grid with a tissue after a few seconds. The grid was dried and investigated with a JEM-2200FS (Jeol, Japan) transmission electron microscope, operated at an acceleration voltage of 200 kV.

Bright field images at increasing magnifications were recorded for a reliable tracking of identical locations of catalyst at the finder grid. Pictures of more than five different platinum loaded carbon aggregates with images showing in total about 40 subregions of carbon aggregates were taken before and after an accelerated aging test. Representative images are shown in this publication. For this purpose, the gold grid was contacted to the glassy carbon disk of the working electrode of the RDE, at which catalyst films are directly deposited in standard electrochemical measurements.

The immobilization of the gold grid on the working electrode was assured with a Teflon cab as shown in Figure S2 in the Supporting Information. The same electrochemical cell and equipment as for the standard electrochemical measurements were utilized, and the experiment was designed analogous to the macroscopic degradation study. A total of 3600 degradation cycles between 0.4 and 1.4 V_{RHE} with a sweep rate of 1 V s^{-1} without rotation was applied for the IL-TEM investigations. IL-TEM was performed already after 3600 degradation cycles, since even longer exposure to the aggressive cycling conditions would hamper the identification of identical locations. The degradation test was done in 0.1 M $HClO_4$, saturated with argon as in the standard electrochemical test. No CO-stripping experiments were performed between the degradation cycles for the IL-TEM study because it is not possible to determine the area of such low amounts of catalyst deposited on the TEM grid. Further details regarding the IL-TEM methodology have been described in previous studies.[16,17]

The particle size distribution was determined from the 2D IL-TEM images. Because the particles are not spherical, the shape was approximated by ellipses. A diameter corresponding to an ideal sphere was calculated for every single particle from the area obtained from the ellipse, and this was used to calculate the average spherical diameter. The total number of particles counted was 1481 particles before and 540 particles remaining in identical locations after the accelerated aging test.

Identical Location Tomography (IL-Tomography). The transmission electron microscope with the aforementioned settings for the imaging was employed for the electron tomography degradation studies, as well. A gold finder grid with a broad mesh (such as NHA2) is necessary to obtain tilting angles as large as possible. The Recorder version 2.32.5.3 program (System in Frontier INC, Japan) was used for the tomography measurements. The images acquisition covered the angular range −74° to +77°. In the range between −45° and +45°, the increment was 2°; for higher tilt angles, to ensure good cross-correlation value, the increment was 1°. Tilting, repositioning, and refocusing were performed automatically after every individual tilt increment. The reconstruction was carried out with Composer version 3.2.10.0 software (System in Frontier INC, Japan) with the Filtered Back Projection (FBP) algorithm. The 3D data were not subjected to any quantitative analysis. The visual treatment of the data was done with Visualizer-Kai Version 1.5.16.0 (System in Frontier INC, Japan). Volume rendering was utilized for the illustration. The accelerated degradation test before and after recording 3D tomography was performed analogously to IL-TEM. The alignment of the two tomograms for the third part of movie 2 (which appears in the HTML version of this paper) was done automatically by the composer software utilized for the illustration. The 3D images before and after degradation show an excellent match.

RESULTS

Electrochemical Measurements. The stability of the catalyst was first estimated with standard electrochemical measurements; particularly, the decline in Pt surface area is quantitatively monitored by adsorption and oxidation of a CO monolayer between the degradation cycles. The CO-stripping curves after certain numbers of accelerated degradation cycles are shown in Figure 1. The voltammograms exhibit all standard

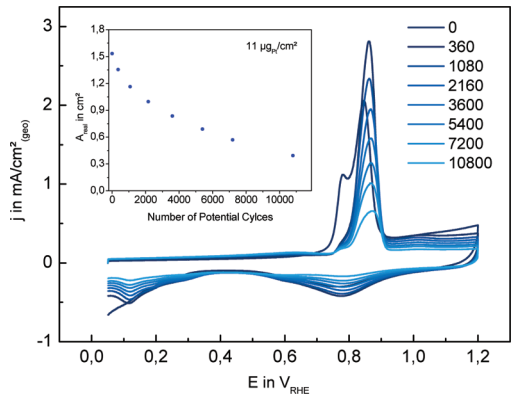

Figure 1. CO-stripping curves at 0.05 V s^{-1} after 0, 360, 1080, 2160, 3600, 5400, 7200, and 10 800 degradation cycles. The intermediate degradation cycles between 0.4 and 1.4 V_{RHE} and 1 V s^{-1} sweep rate are not shown. Inset: Real surface area in square centimeters determined by integration of the CO oxidation peak versus the number of degradation cycles. The illustrated measurement was carried out for an initial catalyst loading of 11 μg_{Pt} cm^{-2}.

features as expected from such CO-stripping experiments.[23] The anodic scan always starts with zero current density in the preignition region between 0.05 and 0.65 V_{RHE} due to the blocking of adsorption or desorption processes on the platinum surface by the adsorbed CO. In particular, the typical features for hydrogen desorption, which would be visible in a corresponding anodic scan without preadsorbed carbon monoxide, are suppressed. At potentials higher than 0.65 V_{RHE}, an oxidation peak due to the oxidative stripping of carbon monoxide from the platinum surface can be seen. After the removal of the adsorbed layer of carbon monoxide, the standard platinum features become visible again: namely, at the end of the anodic scan, platinum oxidation can be identified, because the current density does not decline to zero again after the carbon monoxide oxidation signal. In the cathodic sweep, platinum oxide is reduced in a potential region between 1.0 and 0.55 V_{RHE}. Finally, after the double-layer region between 0.55 and 0.35 V_{RHE}, the features for underpotential hydrogen deposition

dx.doi.org/10.1021/cs300024h | ACS Catal. 2012, 2, 832−843

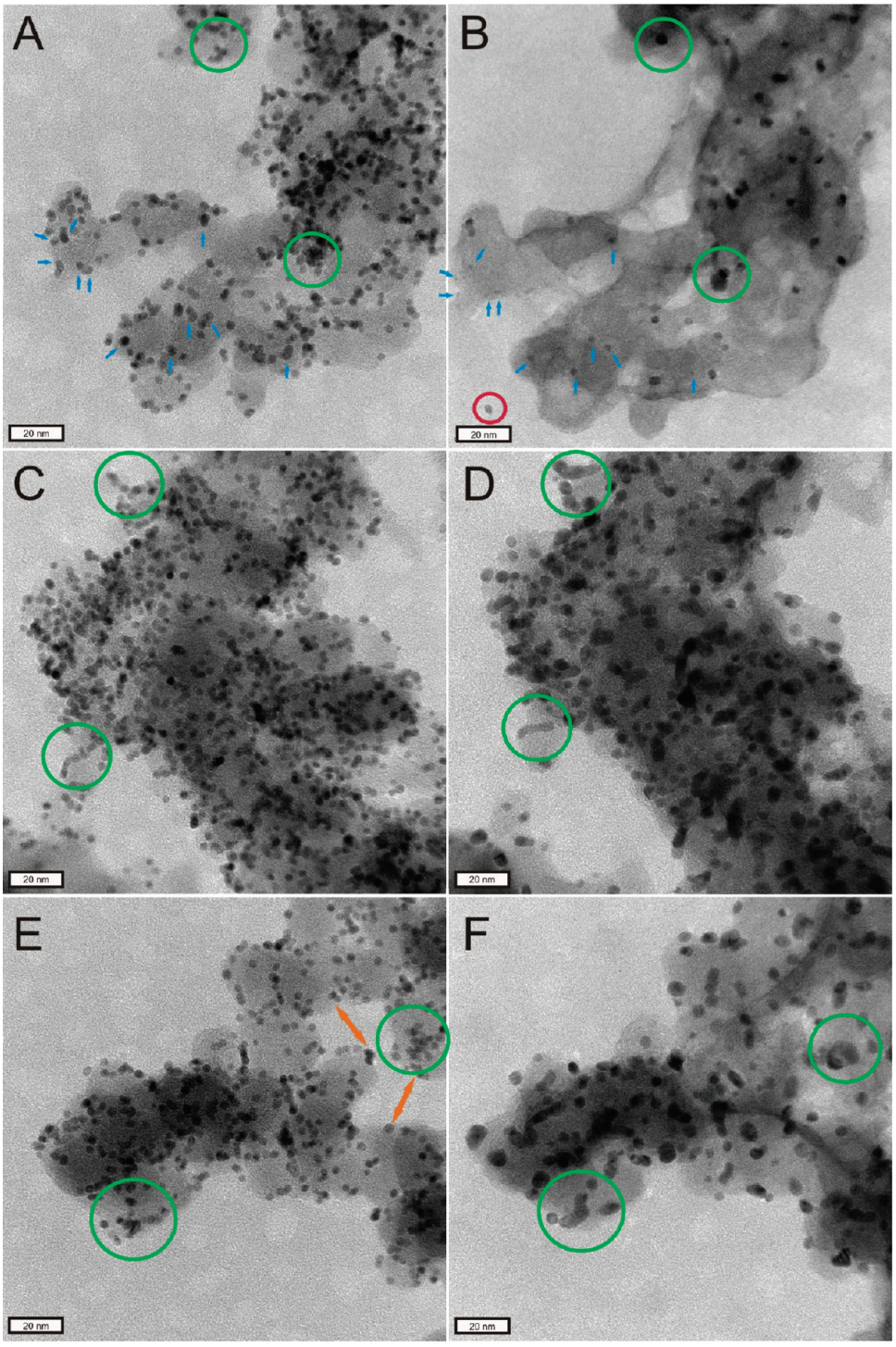

Figure 2. IL-TEM images after 0 (A, C, E) and after 3600 (B, D, F) degradation cycles. Green circles indicate agglomeration, the red circle shows a detached platinum particle, blue arrows point at platinum particles that decrease in size due to dissolution, and orange arrows emphasize massive changes in the support structure.

(H_{UPD}) are observed between 0.35 and 0.05 V_{RHE}, indicating hydrogen adsorption at the platinum surface.

The initial CO-stripping curve (0 degradation cycles), for which carbon impurities have not yet been removed via oxidative cleaning, shows a prepeak for CO oxidation with a maximum at 0.78 V_{RHE} and a main peak with a maximum at 0.85 V_{RHE}. All following CO-stripping curves recorded after starting the degradation procedure no longer contain a significant prepeak. The main peak shape remains the same, and only the area and, therefore, the charge required for CO oxidation are constantly decreasing. The corresponding platinum surface areas calculated from the respective charges[21] are plotted versus the number of degradation cycles in the inset of Figure 1. The material initially possesses an area of 1.53 cm^2 for a platinum loading of 11 μg_{Pt} cm^{-2}, corresponding to an ECSA of 71 m^{-2} g^{-1}. After 3600 cycles, the area decreases significantly to 0.84 cm^{-2} (55%), and after 10 800 cycles, only 0.39 cm^2 (26%) active surface area remains.

dx.doi.org/10.1021/cs300024h | *ACS Catal.* 2012, 2, 832−843

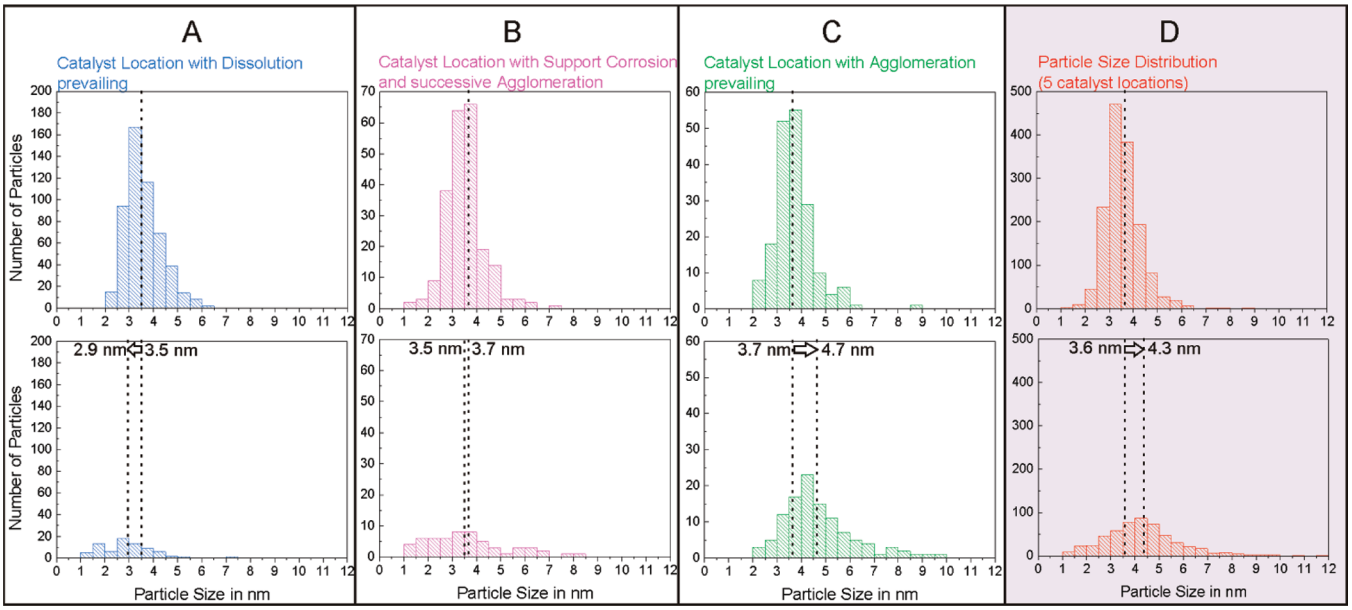

Figure 3. The particle size distribution determined for representative regions of identical catalyst locations are given before (top) and after (bottom) 3600 degradation cycles between 0.4 and 1.4 V_{RHE} at 1 V s^{-1}. The particle size distributions for every single location are headlined with the prevailing degradation mechanism (A–C). An overall particle size distribution obtained from representative regions of five catalyst locations is provided in red (D). The changes in average ideal sphere diameter are illustrated with dashed lines for the single catalyst locations.

Identical Location Transmission Electron Microscopy (IL-TEM). Although the electrochemical experiment above provides important quantitative information about the macroscopic progress of the catalyst deterioration under simulated start–stop conditions, it does not aid in understanding the underlying degradation mechanisms on the nanoscale. Therefore, complementary IL-TEM is employed to gain more insight into the reasons for the Pt surface area loss. Because almost 75% of the catalyst area was lost after 10 800 cycles in the macroscopic electrochemical tests and too severe structural changes are hard to interpret, IL-TEM was performed after only a total of 3600 degradation cycles. Figure 2 shows three different Pt/C catalyst regions before (A, C, E) and after (B, D, F) an accelerated aging test at room temperature. The structural changes are a clear sign of the severe catalyst degradation that has taken place, as was expected from the standard electrochemical measurements.

Most remarkably, an overlap of several different degradation mechanisms can be clearly observed, even at only one catalyst aggregate before and after degradation (Figure 2A and B respectively):

(i) The blue arrows draw attention to particles that decreased in size due to the *dissolution* of platinum particles.
(ii) At the same carbon agglomerate, *detachment* of platinum nanoparticles occurs. The red circle marks one platinum particle that has detached from the support during the start–stop cycling test and was physically trapped next to the catalyst on the coating of the TEM grid.
(iii) The green circles point out two locations with *particle growth*. Especially in the case of the top left circle, it is evident that several small particles have merged into one larger particle.
(iv) The shape of the carbon support has significantly changed due to *carbon corrosion* at the high electrode potentials.

At other catalyst locations, such as in Figure 2C and D, particle growth is more dominant compared with the other degradation processes. The particles in the vicinity of each other highlighted by the green circles seem to form larger particles by agglomeration, which becomes clear from the formation of "stringlike" or "L-shaped" structures. Coarsening is found, in particular in locations with high particle densities, and regions with lower particle densities are often found depleted of particles after electrochemical treatment. The catalyst region in Figure 2E and F again suffers from strong particle growth (e.g., green circles). In addition, significant changes in the structure of the carbon support can be observed in this specific IL-TEM image. The support appears to be more compressed or compact after aging, indicating a loss in structural integrity.

In several locations, one degradation mechanism—namely, particle growth—appears to be dominant for this Pt/Vulcan catalyst under the applied operating conditions. However, indications for an overlap of several degradation mechanisms occurring in parallel are found in most micrographs. It is remarkable that the catalyst locations that are optically not distinguishable exhibit such an inhomogeneous degradation behavior. This is most likely due to the nonhomogeneous composition of the practical support and the concomitant, unequal metal–support interaction, which is, however, hard to detect by analytical means. The overlapping degradation mechanisms as well as inhomogeneous degradation underline the complexity of catalyst degradation under simulated start–stop conditions.

A more quantitative evaluation of the inhomogeneous deterioration of the catalyst based on 2D IL-TEM measurements is provided in Figure 3. The particle size distributions at identical catalyst locations before and after 3600 potential cycles are compared for three specific catalyst locations:

(A) The quantitative evaluation in Figure 3A reveals that the average particle size is decreasing slightly from 3.5 to 2.9 nm in regions where dissolution is a prevailing degradation mechanism (e.g., Figure 2A and B). Because not many large particles are found, agglomeration seems to

dx.doi.org/10.1021/cs300024h | *ACS Catal.* 2012, 2, 832–843

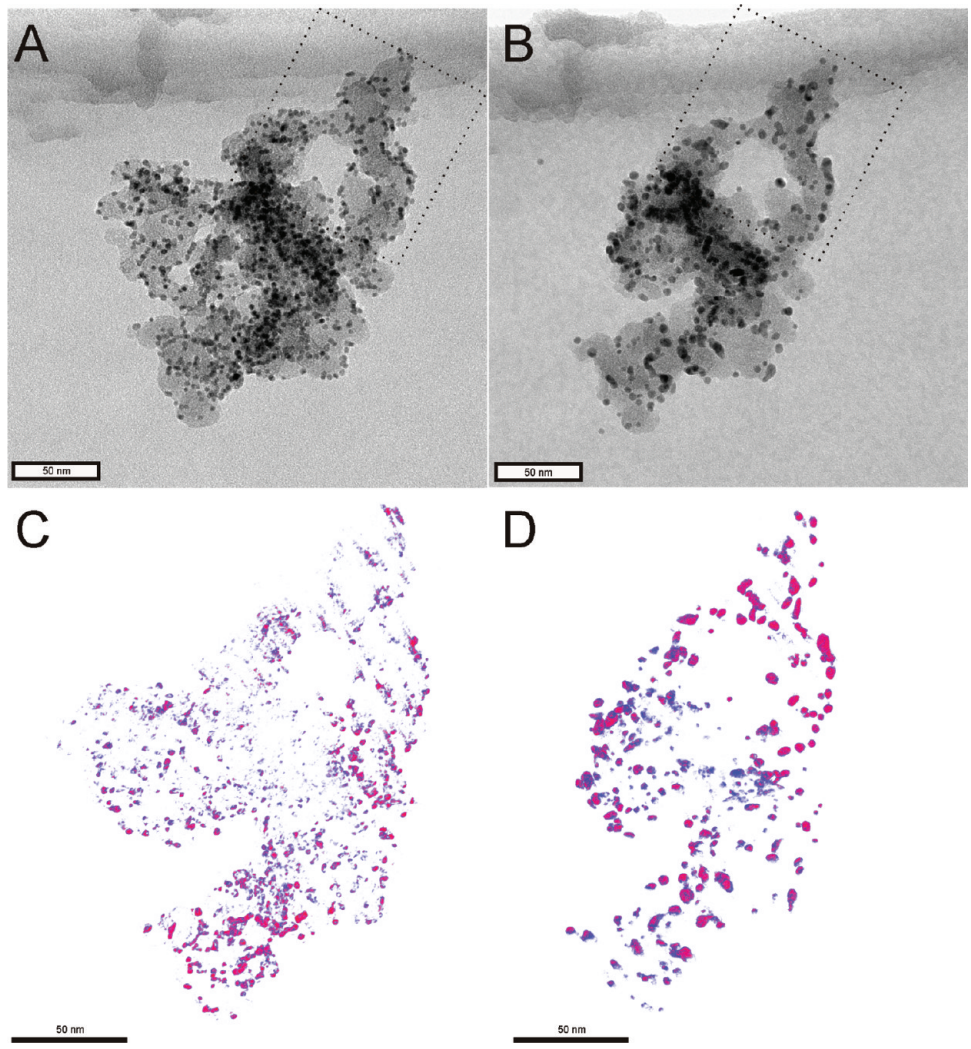

Figure 4. A and B are standard IL-TEM images, C and D are IL-tomography images of the same catalyst location after 0 (A, C) and 3600 (B, D) degradation cycles between 0.4 and 1.4 V_{RHE} with a scan rate of 1 V s^{-1}. The dashed box in A and B highlights the region for which cross sections are shown in Figure 5.

play only a negligible role in the overall platinum area loss in this location.

(B) The particle size distribution shown in Figure 3B corresponds to the degradation for a catalyst location with strong differences in average interparticle distances (for instance, as described later in Figure 6). Massive support corrosion and successive agglomeration is observed in this location. At the same time, dissolution and detachment are clearly observed. Because of these two opposing processes, no significant change in average particle size is taking place. However, the particle size distribution strongly broadens due to an increase in the number of larger and smaller particles while significantly fewer particles of the original size remain.

(C) The changes in particle size distribution in Figure 3C are characteristic for catalyst locations as seen in several micrographs (e.g., Figure 2C and D; E and F) where particle growth is evident. This behavior is observed most often for the catalyst under investigation. The average particle size increases slightly from 3.7 to 4.7 nm, and a log-normal particle size distribution with a tail clearly toward large particles occurs, as expected for agglomeration.[11]

(D) Figure 3D combines the results of evaluations of five different catalyst locations, which were chosen to obtain an overall particle size distribution as representative as possible.

The inhomogeneous degradation behavior visualized in the IL-TEM micrographs and supported by the particle size distributions is most likely due to local differences in the support. The morphology, functionalization, and degree of graphitization of individual carbon particles are decisive for the interaction between platinum particles and support.[24] Further systematic studies will be necessary to resolve these influences in more detail.

Identical Location Tomography (IL-Tomography). TEM micrographs, although most frequently used for the visualization of structures at the nanoscale, have the disadvantage that certain information is lost in the projected 2D image of the real 3D structure. This issue can be circumvented by recording several images at various angles and reconstructing them to provide a stereoscopic vision of the catalyst.[25] In this work, we therefore extend the IL-TEM methodology to IL-tomography and present the first 3D illustrations of an identical catalyst location before and after an accelerated aging test. Figure 4A and B

dx.doi.org/10.1021/cs300024h | ACS Catal. 2012, 2, 832−843

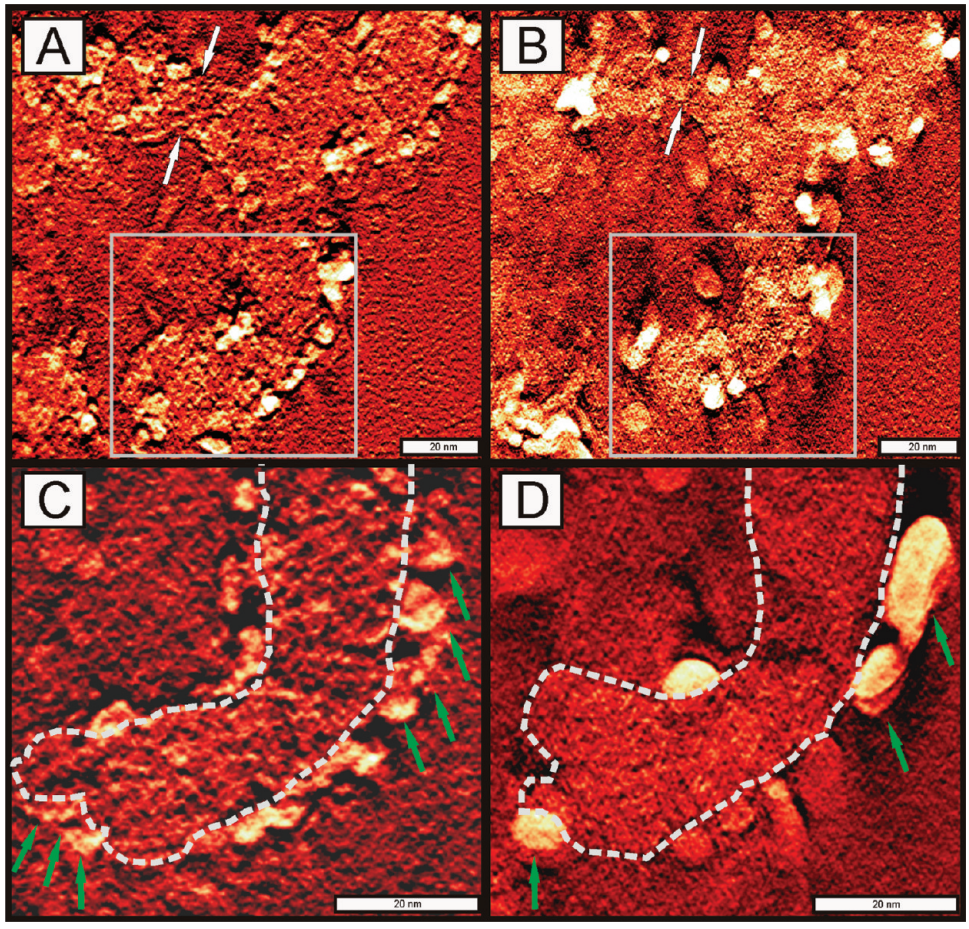

Figure 5. Cross sections through the reconstructed tomograms before (A, C) and after (B, D) 3600 degradation cycles between 0.4 and 1.4 V_{RHE}. A and B are cross sections of the region marked with dashed boxes in Figure 4A and B. The white arrows point out a location in the carbon backbone with thinning of the support due to carbon corrosion. The gray boxes highlight areas for which cross sections are presented in parts C and D. Parts C and D illustrate the carbon support (dashed white lines) and platinum particle agglomeration within the plane (green arrows).

shows standard IL-TEM images of the catalyst, where similar to the observations in Figure 2, severe particle growth can be observed. Furthermore, a change in the structure of the support is evident. A complete fraction of the catalyst aggregate has broken off as an advanced effect of the corrosion of the carbon support. In addition, two platinum particles lying next to the catalyst agglomerate can be seen. Note that these detached particles were not included in the following reconstruction to limit time and effort for computation.

Figure 4C and D are IL-tomography representations of the same catalyst location in the same orientation as seen in A and B. The real 3D impression for the Pt/Vulcan catalyst, however, can be best obtained with the movies available online. Movie 1 (which appears in the HTML version of this paper) shows the sequence of TEM images of the catalyst taken during the tilting procedure between −74° and +77°. The catalyst before degradation on the left side can be seen in parallel to the catalyst after the accelerated aging afterward on the right side. This movie already gives a good three-dimensional impression of the catalyst and the changes in the three-dimensional structure of the support.

On the basis of the images shown in the sequence in movie 1, a reconstruction can be carried out. The result is a 3D representation as provided in movie 2 (which appears in the HTML version of this paper), which first shows the catalyst in its initial state before degradation in blue, rotating 60° clockwise and afterward 60° counterclockwise back to the starting position, and then the appearance of the catalyst after 3600 degradation cycles is illustrated in yellow, again tilting forward and backward for 60°. At the end, an overlap of the previous 3D representations before and after degradation (in blue and yellow) is shown undergoing the same tilting procedure. Although visualization is in principle possible, bad signal-to-noise ratios hamper an appealing and understandable representation of the reconstruction of the support. Thus, the opacity was chosen to only show the platinum particles, which can be illustrated more clearly due to their higher contrast in the TEM. In a first approximation, platinum particles can act as a probe for the carbon support so that an impression of the 3D structure of the support can also be obtained from this representation to a certain degree.

To elucidate the changes in the support more precisely, cross sections derived from the tomograms before and after degradation are presented in Figure 5. The cross sections are taken from the region marked with dashed boxes in Figure 4A and B. Figure 5 allows identification of the support before and after the aging test. For the region presented in Figure 5, only small changes in the carbon structure are visible. Nevertheless, at a few regions of the carbon backbone, thinning due to carbon corrosion is visible (e.g., the region marked with white arrows in Figure 5A and B). The green arrows in Figure 5C and D furthermore indicate agglomeration of platinum particles in the plane under investigation. The platinum nanoparticles are

dx.doi.org/10.1021/cs300024h | *ACS Catal.* 2012, 2, 832−843

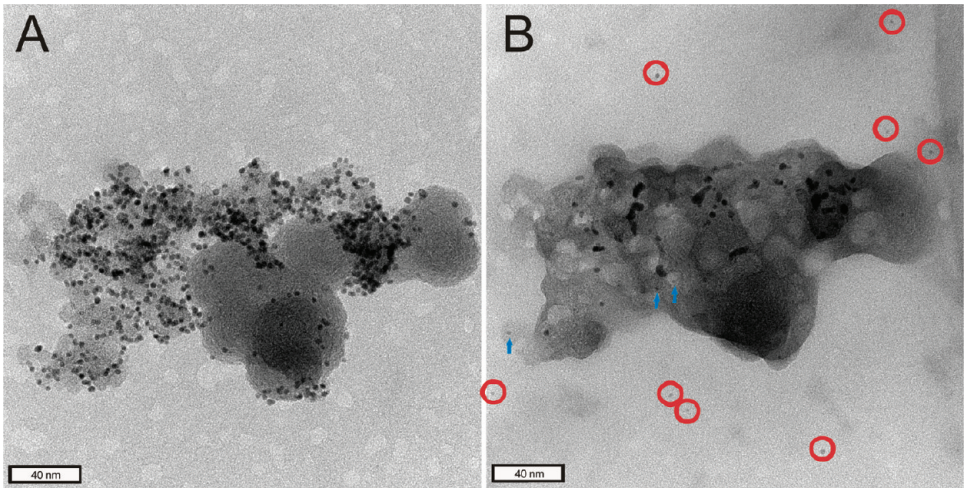

Figure 6. Catalyst location after 0 (A) and 3600 (B) degradation cycles. Severe carbon corrosion as a primary degradation mechanism leads to massive changes in support morphology, and it results in detached platinum particles lying next to the catalyst agglomerate (red circles) as well as agglomeration of particles. In addition, blue arrows point out platinum particles of decreased size due to dissolution.

still located at the carbon support surface so that their accessibility to electrolyte and reaction gases will remain unaltered after degradation.

Significant changes in the platinum nanoparticles can also be observed in movie 2. The growth of platinum particles during degradation becomes more evident from the 3D illustrations (see movies) and is not obscured by overlapping features, as in the 2D projection of standard IL-TEM. Moreover, platinum particles do not appear to be cubooctahedrons, but show an extended contact area with the carbon surface. The three-dimensional representation indicates that contact points of two or more primary carbon particles seem to be regions providing extra stability, because platinum particles or their agglomerates can be found in these protected locations more often after electrochemical treatment than in more exposed positions. The formation of "string-shaped" or even "T-shaped" clusters of platinum particles is clearly present in several locations of the catalyst after degradation. The loss of a complete fraction of the catalyst after electrochemical treatment becomes evident. This is in agreement with the observation of local thinning of the carbon backbone in Figure 5. The missing carbon fraction in movie 2 was connected to the rest of the agglomerate over small "bridges" that are truncated during the aggressive degradation test.

DISCUSSION

An understanding of the influence of operation conditions (such as potential, temperature, pH, humidity, impurities in the system, etc.) as well as the influence of catalyst properties (e.g., platinum particle size distribution, support structure, degree of graphitization, surface functional groups, synthesis methodology, etc.) is indispensable to effectively reduce catalyst degradation. In the following, we will discuss our data obtained under simulated start−stop conditions in light of the most relevant degradation mechanisms debated in the literature.

Dissolution. Platinum is thermodynamically stable toward dissolution in a large pH and potential window; however, according to its Pourbaix diagram,[26] platinum is susceptible to dissolution at potentials higher than 0.85 V_{RHE} at pH values lower than 2 (at 25 °C), which is where PEM cathode fuel cell catalysts are employed. Consequently, dissolved platinum can, for instance, be found in the water stream exiting fuel cells[27] or was shown to redeposit in the ionomer of PEMFCs as a result of reduction with hydrogen permeating the membrane from the anode side.[28−31] Platinum solubility was demonstrated to be highly dependent on the potential value, potential dynamics, temperature, and pH,[8,11,32,33] but the mechanism of platinum dissolution is not completely understood.

In our study, we clearly observe that some platinum particles are decreasing in size, which proves dissolution as one occurring primary degradation mechanism in our system (Figure 2 A and B; Figure 6). This is also evident from the particle size distributions in Figure 3A and B, where in both cases the number of small particles increases. Dissolution is directly observed only at very few locations; however, it might play a more significant role for the overall surface area loss. The timing of taking an IL-TEM image is crucial for the observation of dissolving platinum nanoparticles before they completely vanish, and thus, possibly only a small fraction of all the dissolved particles is captured in each image. In some catalyst regions, only few platinum particles remain after 3600 degradation cycles, particularly for locations of already a low initial platinum particle density, as for instance in Figure 6. Because the significant loss in overall particle number might be the final result not only of dissolution but also of competing particle detachment, a distinction between or even a quantification of the relative contribution of both mechanisms is difficult in many catalyst regions. Moreover, the resolution of TEM for Pt particles on a carbon support is limited so that particles below a certain size are not detectable anymore.

In previous degradation experiments, under identical conditions on a commercial 4.9 nm catalyst (50.6 wt % Pt, Tanaka Kikinzoku Kogyo/TKK, Japan), we observed detachment to be the decisive degradation mechanism,[16] whereas no indication for dissolution was found. Some particles were missing completely, and the others appeared unaltered in shape and size. It has to be emphasized that the nature of the support as well as the platinum loading is quite different in both studies. The catalyst synthesized for the current study has a platinum loading of 20 wt % and a Vulcan XC72 support, whereas the commercial catalyst utilized previously had a platinum loading of 50.6 wt % and a not further described high surface area carbon carrier. Unfortunately, no information was available on the synthesis of the commercial catalyst used in this previous

dx.doi.org/10.1021/cs300024h | ACS Catal. 2012, 2, 832−843

study: neither about possible pretreatment procedures employed on the support nor the catalyst as a whole.

Perez-Alonso et al. were the first to observe platinum nanoparticle dissolution via IL-TEM under slightly milder degradation conditions than in our case (for instance, potential cycling from 0.6 to 1.2 V for 3000 cycles at 0.2 V s^{-1}).[34] The support material was a Vulcan XC72R from Cabot as utilized in the current study; however, the platinum loading of 10 wt % was significantly lower. According to the described synthesis procedure, the material has not been exposed to a heat-treatment procedure, whereas for the material designed for the current study, the highest employed temperature during the synthesis process was 350 °C.

Because the catalyst materials differ in synthesis, platinum loading, pretreatment or even support (see Table S2 in the Supporting Information), a discussion on the differences of the degradation behavior in these three studies is not straightforward. However, it seems that they are at least partly linked to the different particles sizes. Although Perez-Alonso et al. found dissolution to be the only degradation mechanism for their catalyst with an average particle size of 2.3 nm,[34] dissolution is only one of several occurring degradation mechanisms for the catalyst of an average particle size of 3.6 nm investigated here. Interestingly, the same degradation experiments performed on a commercial catalyst of 4.9 nm diameter did not lead to any sign of catalyst dissolution.[16] It seems that under simulated start−stop conditions, catalysts with smaller particle size are significantly more sensitive to dissolution. This has also been derived from other studies without a direct visual confirmation, and it was speculated that the Gibbs−Thomson effect is the reason for this behavior.[8,11] Smaller platinum particles have a higher surface energy, which causes a shift in the equilibrium dissolution potential of platinum to less positive values. On the basis of the model of the kinetics of platinum dissolution by Darling and Meyers,[35] Shao-Horn et al. simulated the influence of the Gibbs−Thomson effect for different particle sizes.[11] Thus, an exponential increase in dissolution rate with decreasing particle size was suggested so that particles of diameters smaller than 2 nm are expected to dissolve orders of magnitude faster than particles with diameters of, for instance, 5 nm, in accordance with the results from the IL-TEM studies.[11] However, further experiments with better comparable catalyst materials and identical testing conditions will be necessary to confirm the influence of particle size on the overall degradation behavior under start−stop conditions and to develop a more quantitative understanding.

Carbon Support Corrosion. In addition to Pt dissolution, the corrosion of the carbon support is the second major primary degradation mechanism. Carbon is thermodynamically susceptible to oxidation to carbon dioxide (standard potential of 0.207 V_{NHE}[26]) in typical fuel cell operation. The reaction is kinetically hindered to a great extent, but is known to be severely enhanced by increasing temperature and potential.[8] Again, the corrosion also strongly depends on the material synthesis, as, for instance, has been demonstrated for the heat pretreatment of the carbon support by the work of Landsman and Luczak.[36]

For the structural properties of standard Vulcan XC72 carbon black materials, it is known that primary carbon particles are the basic building blocks. Usually, these primary carbon particles have a size of ∼20−50 nm that form aggregates of about 100−300 nm, giving an interconnected framework. This framework is important for the formation of an extended meso- and macroporous 3D system, which is crucial for mass-transfer of reactants in a fuel cell. More information about the morphology and porosity of carbon black materials relevant for electrochemical applications can be obtained from the literature.[37]

The carbon particles themselves have been shown to consist of graphene-like sheets. These sheets are well ordered at the surface of the primary particles, but less ordered in the middle of the particles.[37,38] This was suggested to be the reason for the observation of a degradation mechanism, according to which, first, the core of primary particles starts to corrode, leaving a shell-like structure.[39,40] Arenz et al. observed such a mechanism in an IL-TEM study at elevated temperatures and constant potential conditions.[39] In our IL-TEM and IL-tomography investigations on platinum nanoparticles supported on Vulcan XC72, severe carbon corrosion can be observed, even at room temperature. However, neither IL-TEM nor IL-tomography provide indications for the mentioned degradation of primary particles starting from the core. Instead, an example for the loss of a whole fraction of the carbon support from a catalyst aggregate can be observed in movie 2 (see also movie 1 and Figure 4).

The structure of the overall catalyst layer is formed by many such catalyst aggregates containing primary carbon particles. Multiple identical location illustrations (for instance, Figure 2E and F) indicate a contraction of the carbon support, which macroscopically translates into a loss of porosity comparable to the observations of Schulenburg.[41] Because the interconnected porous network of the support is crucial for mass transport of reactants, there is high interest in understanding changes in the support structure during degradation. The support breakdown may result in severe mass-transport limitations, which can strongly reduce the overall fuel cell efficiency. IL-tomography is a very powerful tool to get an impression about the 3D structure of the support before and after degradation. In contrast to the work of Schulenburg,[41] who used electron tomography for in situ studies of comparably large volumes of the catalyst layer directly in a fuel cell, a much higher resolution can be obtained in our approach. Therefore, 3D investigations of changes in single support aggregates and especially changes in platinum nanoparticles before and after an aging test become possible.

Minor changes of the support are visible in most catalyst locations. However, only in about 20−30% of the catalyst images severe carbon degradation is observed (e.g., Figure 2A and B as well as Figure 6). In Figure 6, platinum particles that had detached from the support and particles that are agglomerated are clearly shown as a direct consequence of the severe support oxidation and the concomitant structural and chemical changes. In addition to these massive effects that can easily be recognized by IL-TEM, slight carbon corrosion at the Pt/C interface can also be the origin for initiating such secondary degradation processes. The strong influence of carbon corrosion on the overall degradation behavior emphasizes the importance of studying the effect of the support properties and pretreatment procedures on the resulting degradation pathways.

Ostwald Ripening. Ostwald ripening and agglomeration are the two mechanisms that have been suggested to explain particle growth occurring in fuel cells. Ostwald ripening, which was first applied in this context by Ross,[42] is a secondary degradation mechanism strongly linked to the primary process of platinum dissolution. Small particles dissolve into the electrolyte and shrink, while the dissolved platinum is redeposited on larger platinum particles so that the overall particle size increases.

The driving force for this process is the reduction in surface energy. When dissolution and redeposition are believed to occur mediated through the electrolyte, this mechanism has been referred to as 3D Ostwald ripening. In contrast, when platinum atoms are diffusing along the carbon support from smaller to larger particles, as often observed in high temperature annealing of nanoparticles, this is referred to as 2D Ostwald ripening.[43] A clear distinction between these two pathways is experimentally highly challenging; however, both can be distinguished from agglomeration on the basis of the change in particle size distribution according to theory. A particle size distribution with a tail toward small particle sizes is considered as typical for an Ostwald ripening mechanism, whereas a tail toward large particle sizes is characteristic for agglomeration.[30] Such a log-normal particle size distribution with a tail toward larger particles is observed in this study, as seen in Figure 3C. This offers a strong indication that the particle growth for our catalyst under simulated start–stop conditions is due to agglomeration and not due to Ostwald ripening.

Because of the complexity of the degradation behavior observed in this study, we have to underline that conclusions concerning the degradation mechanism have to be considered as unreliable, if solely on the basis of the change in particle size distribution obtained from post mortem analysis. In a degradation study without utilization of IL-TEM, it can be very difficult or even impossible to reveal overlapping degradation mechanisms.

The results of our IL-TEM and IL-tomography investigations show that both dissolution and particle growth are taking place. Therefore, it cannot be excluded that an Ostwald ripening mechanism is acting. However, specific tracking of certain particles becoming smaller while in their proximity others become larger was not successful. It has to be mentioned that in an IL-TEM study, only very small amounts of catalyst can be deposited on a TEM grid to avoid overlapping of catalyst agglomerates in the images. Therefore, the absolute amount of dissolved platinum species is much lower than expected in a fuel cell, and Ostwald ripening is generally less likely to occur.

Agglomeration. The second possible explanation for the observed particle growth in fuel cells is agglomeration. Migration of platinum particles and successive agglomeration have been suggested to be responsible for coarsening.[44,45] Moreover, platinum particles can also agglomerate due to the corrosion of the support as platinum particles in proximity to each other come into contact when the support shrinks.[8]

It was claimed that "necking" of platinum particles found in TEM images of catalysts in a post mortem analysis of fuel cells can give an indication for agglomeration. "Necking" describes the presence of a bridge with lower diameter between two connected platinum particles.[30] Shao-Horn et al., however, pointed out that "necking" found in TEM images after degradation alone cannot be a proof of agglomeration because it can also be observed in many catalysts without aging tests due to the synthesis procedure.[11] Our tomography movies confirm that "necking" is already present in some locations before degradation. However, we observe further locations with "necking" or comparable features ("string-shaped" and "L-shaped" clusters; e.g., in Figure 2 D and 3 D or even "T-shaped" structures in the IL-tomography movies) where initially no agglomerates but individual particles were present. As a consequence, the particle growth observed in this study can be mainly attributed to agglomeration. It is remarkable that agglomeration is prevalent in catalyst locations with many platinum particles that are already in proximity to each other as unambiguously determined by 3D tomography. Proximity can therefore be a necessary but not a sufficient condition for agglomeration to take place. This is in agreement with the observation of Ruckenstein and Pulvermacher that the rate of particle growth is dependent on particle loading on support.[46]

Starting from the first point of contact, a reshaping of the particles can be observed under the applied potential cycling conditions (Figure 2). In many IL-TEM images, this process is found at different stages; whereas in some locations, particles have just met, and their original shape can still be identified; in other locations, a complete reshaping has already taken place in a particle with lower overall surface area (see also Figure S3 location 1 and 2 in the Supporting Information).

Particle Detachment. Detachment of complete particles from the support, as also observed in this study, has already been reported by our group.[16,17] In this previous study, detachment was the dominating degradation mechanism, but in the current case, detachment is only one of several degradation pathways. In general, detachment results from a weakening of the interaction between the platinum particles and the carbon support; for instance, by corrosion of the carbon directly at the interface. It is remarkable that agglomeration and detachment are observed in parallel because both processes can indicate a weakening of interaction between platinum particles and carbon support.

■ CONCLUSIONS

The degradation behavior of a Pt/Vulcan catalyst was investigated under simulated start–stop conditions. Standard electrochemical investigations of the macroscopic changes in active surface area indicated severe degradation of the catalyst material over a couple of thousands of cycles, and the complexity of the underlying degradation processes was revealed via IL-TEM. In addition, the methodology of IL-TEM was extended to IL-tomography to circumvent the loss of stereoscopic information in standard 2D TEM projections. The illustrations of identical catalyst locations before and after electrochemical treatment thus show the spatial distribution of platinum particles on the support and can be utilized to track morphological changes of the catalyst in three dimensions.

Due to inhomogeneity of the applied support, four different degradation mechanisms can be found at one single catalyst location: dissolution, agglomeration, detachment, and carbon corrosion. These degradation pathways were illustrated to be strongly linked to each other. The primary degradation process of carbon corrosion can, for instance, cause secondary degradation processes such as detachment and agglomeration of platinum particles.

Together with results from previous IL-TEM studies, the importance of particle size as well as the catalyst pretreatment on the degradation mechanism was emphasized. Namely, a particle size effect for the mechanism of platinum nanoparticle dissolution is supported by our results. Furthermore, "string-shaped", "L-shaped", or "T-shaped" platinum clusters were identified at catalyst locations after degradation where

single particles had been found before, providing proof for agglomeration.

■ ASSOCIATED CONTENT

Supporting Information

More detailed information about the catalyst material and additional information as noted in the text. This material is available free of charge via the Internet at http://pubs.acs.org.

■ AUTHOR INFORMATION

Corresponding Author

*Phone: +49 211 6792 160. Fax: +49 211 6792 218. E-mails: (J.C.M.) meier@mpie.de, (K.J.J.M.) mayrhofer@mpie.de.

Author Contributions

The electrochemical degradation experiments, TEM and tomography measurements and the tomography reconstruction were designed and performed by Josef Meier. The catalyst was synthesized and chemically characterized by Carolina Galeano. Ioannis Katsounaros and Angel Topalov assisted with the electrochemical measurements. The manuscript was written by Josef Meier. All authors contributed to scientific discussions and assisted with the writing of the manuscript.

Notes

The authors declare no competing financial interest.

■ ACKNOWLEDGMENTS

We thank Dr. C. Weidenthaler for XPS measurements performed at the Max-Planck-Institut für Kohlenforschung in Mülheim. Josef C. Meier acknowledges financial support by the Kekulé Fellowship from the Fonds der Chemischen Industrie (FCI).

■ REFERENCES

(1) Kinoshita, K. *J. Electrochem. Soc.* **1990**, *137*, 845−848.
(2) Mayrhofer, K. J. J.; Blizanac, B. B.; Arenz, M.; Stamenkovic, V. R.; Ross, P. N.; Markovic, N. M. *J. Phys. Chem. B* **2005**, *109*, 14433−14440.
(3) Nesselberger, M; Ashton, S.; Meier, J. C.; Katsounaros, I.; Mayrhofer, K. J. J.; Arenz, M. *J. Am. Chem. Soc.* **2011**, *133*, 17428−17433.
(4) Gasteiger, H. A.; Kocha, S. S.; Sompalli, B.; Wagner, F. T. *Appl. Catal., B* **2005**, *56*, 9−35.
(5) Stamenkovic, V. R.; Fowler, B.; Mun, B. S.; Wang, G.; Ross, N. P.; Lucas, C. A.; Markovic, N. M. *Science* **2007**, *315*, 493−497.
(6) Stamenkovic, V. R.; Mun, B. S.; Arenz, M.; Mayrhofer, K. J. J.; Lucas, C. A.; Wang, G.; Ross, N. P.; Markovic, N. M. *Nat. Mater.* **2007**, *6*, 241−247.
(7) Greeley, J.; Stephens, E. L.; Bondarenko, A. S.; Johansson, T. P.; Hansen, H. A.; Jaramillo, T. F.; Rossmeisl, J.; Chorkendorff, I.; Nørskov, J. K. *Nat. Chem.* **2009**, *1*, 552−556.
(8) Mench, M. M.; Kumbar, E. C.; Veziroglu, T. N. *Polymer Electrolyte Fuel Cell Degradation*; Academic Press Elsevier: Waltham, 2012.
(9) Zhang, S.; Yuan, X.; Wang, H.; Mérida, W.; Zhu, H.; Shen, J.; Wu, S.; Zhang, J. *Int. J. Hydrogen Energy* **2009**, *34*, 388−404.
(10) Borup, R.; Meyers, J.; Pivovar, B.; Kim, Y. S.; Mukundan, R.; Garland, N.; Myers, D.; Wilson, M.; Garzon, F.; Wood, D.; Zelenay, P.; More, K.; Stroh, K.; Zawodinski, T.; Boncella, J.; McGrath, J. E.; Inaba, M.; Miyatake, K.; Hori, M.; Ota, K.; Ogumi, Z.; Miyata, S.; Nishikata, A.; Siroma, Z.; Uchimoto, Y.; Yasuda, K.; Kimijima, K.; Iwashita. *Chem. Rev.* **2007**, *107*, 3904−3951.
(11) Shao-Horn, Y.; Sheng, W. C.; Chen, S.; Ferreira, P. J.; Holby, E. F.; Morgan, D. *Top. Catal.* **2007**, *46*, 285−305.
(12) Zhang, S.; Yuan, X.; Hin, J. N. C.; Wang, H.; Friedrich, K. A.; Schulze, M. *J. Power Sources* **2009**, *194*, 588−600.
(13) Shao, Y.; Yin, G.; Gao, Y. *J. Power Sources* **2007**, *171*, 558−566.
(14) Gu, W.; Carter, R. N.; Yu, P. T.; Gasteiger, H. A. *ECS Trans.* **2007**, *11*, 963−973.
(15) Kinoshita, K.; Lundquist, J. T.; Stonehart, P. *J. Electroanal. Chem.* **1973**, *48*, 157−166.
(16) Mayrhofer, K. J. J.; Meier, J. C.; Ashton, S. J.; Wiberg, G. K. H.; Kraus, F.; Hanzlik, M.; Arenz, M. *Electrochem. Commun.* **2008**, *10*, 1144−1147.
(17) Mayrhofer, K. J. J.; Ashton, S. J.; Meier, J. C.; Wiberg, G. K. H.; Hanzlik, M.; Arenz, M. *J. Power Sources* **2008**, *185*, 734−739.
(18) Jia, C.-J.; Schüth, F. *Phys. Chem. Chem. Phys.* **2011**, *13*, 2457−2487.
(19) Yan, X.; Liu, H.; Liew, K. Y. *J. Mater. Chem.* **2001**, *11*, 3387−3391.
(20) Hartl, K.; Hanzlik, M.; Arenz, M. *Energy Environ. Sci.* **2011**, *4*, 234−238.
(21) Topalov, A. A.; Katsounaros, I.; Meier, J. C.; Klemm, S. O.; Mayrhofer, K. J. J. *Rev. Sci. Instrum.* **2011**, *82*, 114103.
(22) Mayrhofer, K. J. J.; Strmcnik, D.; Blizanac, B. B.; Stamenkovic, V.; Arenz, M.; Markovic, N. M. *Electrochim. Acta* **2008**, *53*, 3181−3188.
(23) Arenz, M.; Mayrhofer, K. J. J.; Stamenkovic, V.; Blizanac, B. B.; Tomoyuki, T.; Ross, P. N.; Markovic, N. M. *J. Am. Chem. Soc.* **2005**, *127*, 6819−6829.
(24) Grothausmann, R.; Zehl, G.; Manke, I.; Fiechter, S.; Bogdanoff, P.; Dorbandt, I.; Kupsch, A.; Lange, A.; Hentschel, M. P.; Schumacher, G.; Banhart, J. *J. Am. Chem. Soc.* **2011**, *133*, 18161−18171.
(25) Gontard, L. C.; Dunin-Borkowski, R. E.; Ozkaya, D. *J. Microsc.* **2008**, *232*, 248−259.
(26) Pourbaix, M. *Atlas of Electrochemical Equilibria in Aqueous Solutions*, 2nd English ed.; Association of Corrosion Engineers: Houston, TX, 1974.
(27) Mukerjee, S.; Srinivasan, S. In *Handbook of Fuel Cells − Fundamentals, Technology and Applications*; Vielstich, W., Lamm, A., Gasteiger, H., Eds.; John Wiley & Sons: Chichchester, UK, 2003; Vol. 3; p 503.
(28) Aragane, J.; Murahashi, T.; Odaka, T. *J. Electrochem. Soc.* **1988**, *135*, 844−850.
(29) Aragane, J.; Urushibata, H.; Murahashi, T. *J. Appl. Electrochem.* **1996**, *26*, 147−152.
(30) Shao-Horn, Y.; Ferreira, P. J.; la O', G. J.; Morgan, D.; Gasteiger, H. A.; Makharia, R. *ECS Transactions* **2006**, *1*, 185−195.
(31) Ferreira, P. J.; la O', G. J.; Shao-Horn, Y.; Morgan, D.; Makharia, R.; Kocha, S.; Gasteiger, H. A. *J. Electrochem. Soc.* **2005**, *152*, A2256−A2271.
(32) Mitsushima, S.; Koizumi, Y.; Uzuka, S.; Ota, K.-I. *Electrochim. Acta* **2008**, *54*, 455−460.
(33) Inzelt, G.; Berkes, B.; Kriston, Á. *Electrochim. Acta* **2010**, *55*, 4742−4749.
(34) Perez-Alonso, F. J.; Elkjær, C. F.; Shim, S. S.; Abrams, B. L.; Stephens, I. E. L.; Chorkendorff, I. *J. Power Sources* **2011**, *196*, 6085−6091.
(35) Darling, R. M.; Meyers, J. P. *J. Electrochem. Soc.* **2003**, *150*, A1523−A1527.
(36) Landsman, D.; Luczak, F. J. *Catalyst Studies and Coating Technologies*; John Wiley & Sons: West Sussex, England, 2003; Vol. 4.
(37) Kinoshita, K. *Carbon: Electrochemical and Physicochemical Properties*; Wiley: New York, 1988.
(38) Wissler, M. *J. Power Sources* **2006**, *156*, 142−150.
(39) Gruver, G. A. *J. Electrochem. Soc.* **1978**, *125*, 1719−1720.
(40) Schlögl, K.; Mayrhofer, K. J. J.; Hanzlik, M.; Arenz, M. *J. Electroanal. Chem.* **2011**, *662*, 355−360.
(41) Schulenburg, H.; Schwanitz, B.; Linse, N.; Scherer, G. G.; Wokaun, A.; Krbanjevic, J.; Grothausmann, R.; Manke, I. *J. Phys. Chem. C* **2011**, *115*, 14236−14243.
(42) Ross, P. N. In *Catalyst Deactivation*; Petersen, E. E., Bell, A. T., Eds.; Marcel Dekker: New York, 1987; p 165.
(43) Bett, J. A. S.; Kinoshita, K.; Stonehart, P. *J. Catal.* **1976**, *41*, 124−133.

(44) Wilson, M. S.; Garzon, F. H.; Sickafus, K. E.; Gottesfeld, S. *J. Electrochem. Soc.* **1993**, *140*, 2872−2876.
(45) Tada, T.; Kikinzoku, T. In *Handbook of Fuel Cells − Fundamentals, Technology and Applications*; Vielstich, W., Lamm, A., Gasteiger, H., Eds.; John Wiley & Sons: Chichchester, UK, 2003; Vol. 3; p 481.
(46) Ruckenstein, E.; Pulvermacher, B. *J. Catal.* **1973**, *29*, 224−245.